Supplementary Information for "On performance of thin-film meso-structured perovskite solar cell through experimental analysis and device simulation"

F. Bonnín-Ripoll[1], Ya. B. Martynov[2], R. G. Nazmitdinov [3,4], K. Tabah[5], C. Pereyra [5], M. Lira-Cantú[5], G. Cardona[6], R. Pujol-Nadal[1]

[1] *Departament d'Enginyeria Industrial i Construcció, Universitat de les Illes Balears, E-07122 Palma, Spain.*

[2] *State Scientific-Production Enterprise "Istok" Fryazino, Russia.*

[3] *Bogoliubov Laboratory of Theoretical Physics, Joint Institute for Nuclear Research, 141980 Dubna, Moscow region, Russia.*

[4] *Dubna State University, 141982 Dubna, Moscow region, Russia.*

[5] *Catalan Institute of Nanoscience and Nanotechnology (ICN2), CSIC and the Barcelona Institute of Science and Technology (BIST), Building ICN2, Campus UAB, E-08193 Bellaterra, Barcelona, Spain.*

[6] *Departament de Matemàtiques, Universitat de les Illes Balears, E-07122 Palma, Spain.*

S1. Device Characteristics

The device fabrication and the experimental work, presented in this paper, have been carried out at the facilities of the Institut Català de Nanociència i Nanotecnologia (ICN2) in collaboration with the Nanomaterials for Photovoltaics Energy research group. The perovskite solar cells have been fabricated with the FTO/c-TiO_2/mp-TiO_2/Perovskite/Spiro-OMeTAD/Au configuration using multi-cationic perovskite. Each of these materials has its own synthesis and deposition process; all fabrication details are discussed in (1). Example of final samples is shown in Fig.S1.

Email address: f.bonnin@uib.cat (F. Bonnín-Ripoll[1])

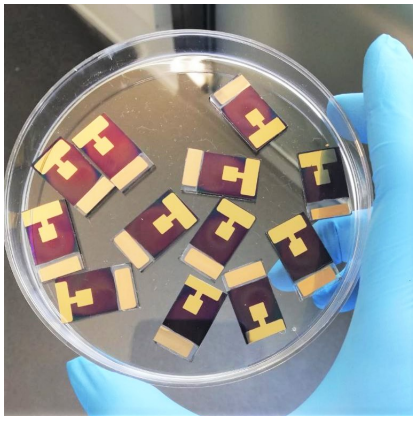

Figure S1: Image of the perovskite solar cell samples at the final stage of the manufacturing process.

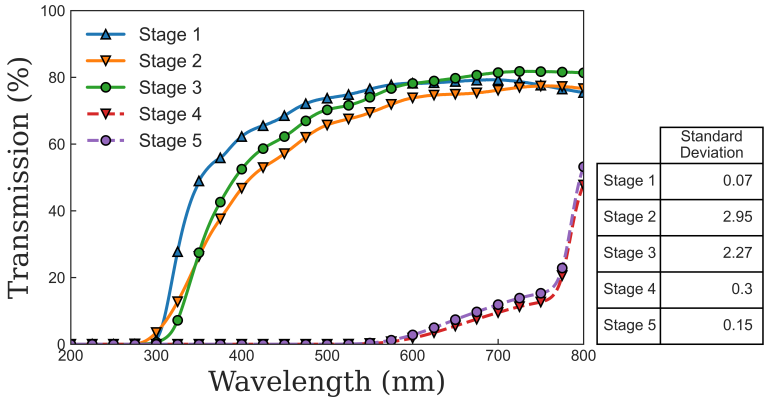

	Standard Deviation
Stage 1	0.07
Stage 2	2.95
Stage 3	2.27
Stage 4	0.3
Stage 5	0.15

Figure S2: Mean values and standard deviations of the optical transmittance measurements for each manufacturing stages of the perovskite solar cell. Standard deviations have been calculated at each wavelength for six experimental samples (see also the main text).

Transmittance

Transmittance measurements have been done by means of the UV-Vis CARY 4000 spectrophotometer at normal incidence, using the solid sample holder accessory. The incident radiation consists of $200-800$ nm wavelength range of the optical spectrum. The results of the mean value of the optical transmittance measurements for each stage as a function of the wavelength are shown in Fig.S2. Our measurements make manifest that it is enough to fabricate six samples at each stage to obtain a reliable result for the mean

value. Additionaly, we indicate the standard deviation from the mean value for each curve, corresponding to each stage. The largest deviations are obtained for the c-TiO_2 and mp-TiO_2 depositions (stages 2 and 3, respectively). Noteworthy, up to now there is no any available criterium in literature regarding definition of the effective border line between c-TiO_2 and mp-TiO_2 depositions. In fact, one of our goals is to propose such the effective methodology.

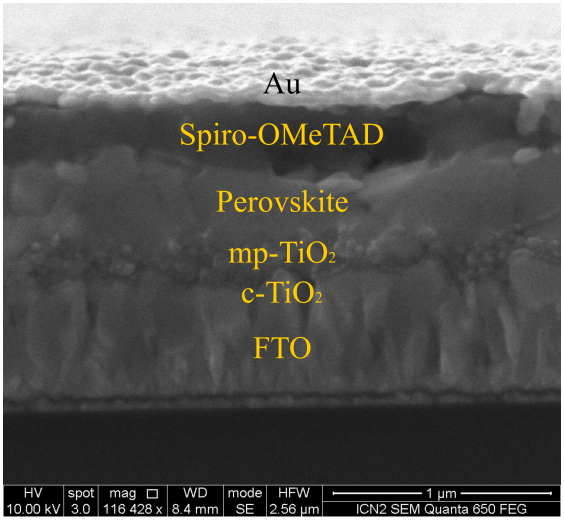

Figure S3: Cross-section image of the samples, obtained by means of the scanning electron microscope. It is quite visible the degree of the gold layer roughness. The extracted approximate thickness of each layer is presented in Table S1.

Layer Thicknesses

The approximate thickness of each material layers has been estimated using scanning electron microscopy (SEM) techniques (see Fig.S3). These images are essential for modelling the PSC, since each layer thickness assesment is a key parameter in the following model calculations. The heterogeneity observed in the layer thicknesses is due to the experimental process itself, subject to variations in the initial conditions, the experience and skill of the technician, the correct stoichiometric balance of the compounds, etc. The less accuracy for the estimation of the c-TiO_2 layer thickness is due to its extension diapason in the range of a few tens of nanometers.

Note that the substrate is formed by four different materials. The thickness of each component in the compound is provided by the manufacturer

Material	Thicknesses (nm)
SiO_2	10-30
SnO_2	10-30
FTO	500-600
c-TiO_2	10-30
mp-TiO_2	180-300
Perovskite	400-550
Spiro-OMeTAD	200-250

Table S1: Thickness range of the material layers present in the PSC samples measured by scanning electron microscopy.

itself: 2.2 mm of glass, 25 nm of SnO_2 and SiO_2, and 540 nm of FTO. Even so, in the images (see Fig.S3) it can be seen that the FTO is not completely homogeneous. Consequently, we consider a certain range of thicknesses, in which the calculations for the characterization are carried out. From the images obtained by SEM, the thickness ranges considered for the materials in the successive calculations, are shown in Table S1.

S2. Detailed elaboration of thickness configuration

In order to fit theoretical and experimental transmittances, a concrete thickness configuration of the PSC structure is needed. Since scanning electronic microscope images show that the thicknesses of the layers is not completely homogeneous, we must consider a range between which each layer thickness lies. Before to resolve this problem we have to analyse the optical properties of each layer.

One of the most common theoretical tools used to analyse the optical properties of complex solar systems with a high accuracy is the so called Monte-Carlo ray tracing simulation. It consists of a set of techniques that determine the path of light through matter in a three-dimensional environment with computer simulations (2). We implement in our approach the Monte-Carlo ray tracing technique, adding the transfer-matrix method (TMM) to characterize the optical response of the PSC with the aid of the ray trace OTSun python package (3; 4; 5). In order to carry out simulations in a simpler and faster way, first, we use the TMM only to determine the thicknesses configuration. Based on the results discussed hereafter, the OTSun will be used (see the main text) as the subsequent step where more accurate calcu-

lations are needed. Consequently, using the ranges shown in Table S1, each possible configuration is considered to provide the transmittance with the aid of the TMM calculation, to obtain those that are closer to the experimental curves. To reach our goal we introduce the root mean square error (RMSE) of each thickness configuration for a given material thickness

$$RMSE = \frac{1}{N}\sqrt{\sum_{\lambda=300}^{\lambda=800}[T^{exp}(\lambda) - T^{th}(\lambda)]^2}\,. \tag{1}$$

Here, N is the total number of wavelength steps; the step is equal to 1 nm in all cases; $T^{exp}(T^{th})$ is the experimental (theoretical) optical transmittance. Hereafter, it is convenient to introduce the range limits of the thickness variation for each layer as [a,b] (in nm).

First, we carry out the calculations for the stage 1. To this aim we consider the following thicknesses: [10,30] for SnO_2 and SiO_2; [500, 600] for FTO. As a result, we choose those configurations that lie within 1% of the lowest RMSE.

Next, we proceed to the stage 2 (repeating similar calculations), using the range limits obtained from the stage 1: [10,20] for SnO_2 and SiO_2; [550,600] for FTO; [10,30] for c-TiO_2. These calculations reduce the starting range limits to [10,16], [14,20], [550,600], [22,30] for SnO_2, SiO_2, FTO, c-TiO_2, respectively.

Afterwards, we move to the stage 3, where both the thickness and the porosity of the mp-TiO_2 are added to the system. An initial sweep is made considering the previous ranges plus the mp-TiO_2 [180,300] layer and its porosity considered between 1% and 50%. Considering the configurations that lie within 1% of the lowest RMSE, the material thicknesses are varied in the following intervals: [10,12] for SnO_2; [14,18] for SiO_2; [555,580] for FTO; [23,25] for c-TiO_2; [200,300] for mp-TiO_2, and its porosity reduced to the 10%–20% range.

From our previous experience (see details in (6; 7)) it follows that small changes in layer thicknesses (in order of a few nanometers) at the stage 2 do not affect the optical transmittance of the device. Therefore, we choose the mean values 11, 16, 565, and 24 nm (associated with SnO_2, SiO_2, FTO, c-TiO_2 layer thickness, respectively), which are defined within the ranges imposed by the stage 3. By fixing these values, we also reduce significantly the calculation time, enabling us to explore the mesoporous material and its subsequent influence on the properties of the absorbing layer.

We recall that the stage 4 includes the perovskite layer considered in the [400,550] interval, while keeping the variability of the porosity and thickness of the mp-TiO_2 layer as mentioned above. Since there is a complex interplay of the transmittance through the mp-TiO_2 layer and its effect on the transmittance through the perovskite, we consider the ranges of three parameters simultaneously: i) the mp-TiO_2 layer thickness; ii) its porosity; iii) the perovskite thickness within 5% of the lowest RMSE selection. As a result, we obtain that: the mp-TiO_2 porosity oscillates between 10% and 20%, while its thickness between 260 and 300 nm; the perovskite layer thickness oscillates between 450 and 500 nm.

In the stage 5 the Spiro-OMeTAD layer is added with a thickness defined in [200,250] nm interval. Our calculations yield that the configurations within 5% of the lowest RMSE lie in the following interval (in nm): [270,300] for the mp-TiO_2 layer; the porosity is defined between 15% and 20%; [450,470] for the perovskite layer; [200, 250] for the Spiro-OMeTAD layer.

Notice that the configurations that fit better the optical behaviour of the experimental samples are not necessarily those that fit better the electronic properties of the experimental samples. Consequently, our analysis is supplemented by one more parameter: the short-circuit current J_{sc}. Therefore, considering the ranges of parameters for each material obtained under the previous procedure and making them less restrictive, we proceed to the calculations of the short-circuit current J_{sc}, which will involve adding the gold metal layer to the system. Again, we have to vary the discussed parameters within the above limits (see below). Taking this fact into account, the maximum possible photocurrent is calculated in the assumption that all absorbed photons generate electron and holes and contribute to the current (8). In an efficient PSC this current is closely related to the short-circuit current, J_{sc}. As a result, to reach a consistently between optical and electronic properties we calculate the short-circuit current for every configuration, taking into account that the mean value of the measured current $J_{sc} = 20.07$ mA/cm^2 (see details in the main text).

We recall that all the effects regarding the radiation-matter interaction mentioned above, are needed to elucidate the number of absorbed photons inside active materials. To this aim the photogeneration rate G of the creation of pairs of electrons/holes should be considered a position-dependent function within the material thickness. To this aim we employ the method proposed by Ball et al. (9) and the TMM library (10) to calculate the short-

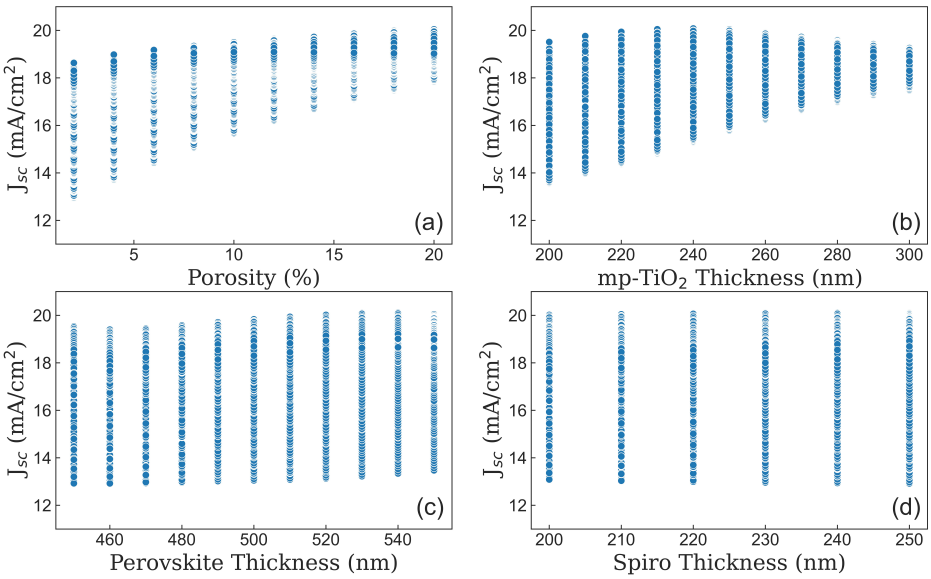

Figure S4: The short-circuit current J_{sc} as a function of mp-TiO_2 porosity (a), mp-TiO_2 thickness (b), perovskite thickness (c) and Spiro-OMeTAD thickness (d).

circuit current J_{sc} as:

$$J_{sc} = q \int G(\lambda, z) d\lambda dz \,, \tag{2}$$

where q is the electron charge, and z is the depth from the semiconductor surface.

Turning to the calculation details of the discussed procedure, first, we fix the multilayer glass thicknesses at 11, 16, 565 (nm) for SnO_2, SiO_2, FTO, respectively; and 24 nm for c-TiO_2. Second, it is observed that the photocurrent is very sensitive to the thickness and porosity of the mp-TiO_2 layer. Indeed, it should be noted that at stages 2 and 3 that correspond to the deposition of the c-TiO_2 and the mp-TiO_2 layers, respectively, a standard deviation 10 times higher relative to those for other stages (see Fig.S2). Including the J_{sc} calculations to the RMSE result obtained from the transmittance fitting, we weakend the boundaries found above, in particularly, for the porosity and for the mp-TiO_2 layer thickness. Consequently, we vary the porosity and thickness of the mp-TiO_2 layer (from 2% to 20%, from 200 to 300 nm, respectively); the perovskite thickness (from 450 to 550 nm); the Spiro-OMeTAD thickness (from 200 to 250 nm). As a result, we do calculations by varying the following parameters:

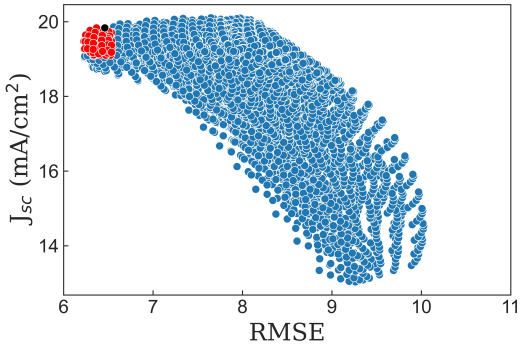

Figure S5: The short-circuit J_{sc} as a function of the RMSE, calculated by fitting the experimental and theoretical transmittance of stage 5. The optimal configurations (red solid points) are located in the range of $\pm 5\%$ deviation from the experimental value of the short-circuit current. Black point corresponds to the selected case, used for comparison of experimental and theoretical J-V characteristics (see main text).

1. porosity takes 10 possible values;
2. mp-TiO_2 thickness takes 11 possible values;
3. perovskite thickness takes 11 possible values;
4. Spiro-OMeTAD thickness takes 6 possible values,

i.e. we have a set of $10 \times 11 \times 11 \times 6 = 7260$ combinations determined by the parameters variations. Altogether the chosen parameters provide the basis for the calculation of the set J_{sc} values (see Fig.S4).

Among all the possible configurations, we have selected those that hold the following criteria: i) be $\leq |5|\%$ with respect to the experimental value of the short-circuit current J_{sc}; ii) be $\leq 5\%$ of the lowest RMSE (red region in Fig.S5). From this selection, the configuration with the highest J_{sc} has been chosen denoted by the black point on Fig.S5.

The results for the short-circuit current J_{sc} demonstrate: i) its less sensitivity to the variation of the perovskite and Spiro-OMeTAD thicknesses; ii) while the close correspondence to the experimental value of the short-circuit current J_{sc} takes place at the thickness 240 nm and the porosity value = 20% of the mp-TiO_2 layer.

Summarising, according to our analysis the theoretical configuration, chosen to model the experimental samples, consists of the following layer thicknesses (in nm): 11 (SiO_2), 16 (SnO_2), 565 (FTO), 24 (c-TiO_2), 240 (mp-TiO_2, the porosity = 20%), 500 (Perovskite), 250 (Spiro-OMeTAD). This configuration is obtained as a result of optimization of the optical transmittance of

the device configuration at the value of the short-circuit current $J_{sc} = 19.83$ mA/cm^2.

[1] H. Xie, Z. Wang, Z. Chen, C. Pereyra, M. Pols, K. Gałkowski, M. Anaya, S. Fu, X. Jia, P. Tang, D. J. Kubicki, A. Agarwalla, H. S. Kim, D. Prochowicz, X. Borrisé, M. Bonn, C. Bao, X. Sun, S. M. Zakeeruddin, L. Emsley, J. Arbiol, F. Gao, F. Fu, H. I. Wang, K. J. Tielrooij, S. D. Stranks, S. Tao, M. Grätzel, A. Hagfeldt, M. Lira-Cantu, Decoupling the effects of defects on efficiency and stability through phosphonates in stable halide perovskite solar cells, Joule 5 (5) (2021) 1246–1266. doi:10.1016/J.JOULE.2021.04.003.

[2] J. Bos-Coenraad, L. Bunthof, J. Schermer, Scientrace: An open source, programmable 3D ray tracer, Solar Energy 155 (2017) 1188–1196. doi:10.1016/J.SOLENER.2017.07.003.

[3] G. Cardona, R. Pujol-Nadal, OTSun Python Package (2018).
URL `https://github.com/bielcardona/OTSun`

[4] OTSunWebApp (2018).
URL `http://otsun.uib.es/otsunwebapp`

[5] F. Bonnín-Ripoll, G. Cardona, R. Nadal-Pujol, Tutorial 2 OTSun Web App (2018).
URL `https://github.com/bielcardona/OTSun/blob/master/OTSunWebApp/Tutorial_2_1e_OTSun_WebApp.pdf`

[6] F. Bonnín-Ripoll, Y. B. Martynov, G. Cardona, R. G. Nazmitdinov, R. Pujol-Nadal, Synergy of the ray tracing+carrier transport approach: On efficiency of perovskite solar cells with a back reflector, Solar Energy Materials and Solar Cells 200 (2019) 110050. doi:10.1016/j.solmat.2019.110050.

[7] F. Bonnín-Ripoll, Y. B. Martynov, R. G. Nazmitdinov, G. Cardona, R. Pujol-Nadal, On the efficiency of perovskite solar cells with a back reflector: effect of a hole transport material, Physical Chemistry Chemical Physicsdoi:10.1039/D1CP03313A.

[8] J. García-Cañadas, F. Fabregat-Santiago, H. J. Bolink, E. Palomares, G. Garcia-Belmonte, J. Bisquert, Determination of electron and hole

energy levels in mesoporous nanocrystalline TiO_2 solid-state dye solar cell, Synthetic Metals 156 (14) (2006) 944–948.

[9] J. M. Ball, S. D. Stranks, M. T. Hörantner, Sven Hüttner, Wei Zhang, E. J. W. Crossland, Ivan Ramirez, Moritz Riede, M. B. Johnston, R. H. Friend, H. J. Snaith, Optical properties and limiting photocurrent of thin-film perovskite solar cells, Energy & Environmental Science 8 (2) (2015) 602–609. doi:10.1039/C4EE03224A.

[10] S. Byrnes, tmm 0.1.7 : Python Package Index (2017).